The possible dual nature of the asteroid (12499) 1998 FR47

G. Borisov[1,2] , **N. Todorović**[3], **E. Vchkova-Bebekovska**[4],
A. Kostov[1] **and G. Apostolovska**[4]

[1] *Institute of Astronomy with NAO, Bulgarian Academy of Sciences, 72
Tsarigradsko Chaussée Blvd, BG-1784, Sofia, Bulgaria, (E-mail:
gborisov@astro.bas.bg)*

[2] *Armagh Observatory and Planetarium, College Hill, Armagh BT61 9DG,
Northern Ireland, United Kingdom*

[3] *Astronomical Observatory, Volgina 7, Belgrade, 11060, Serbia*

[4] *Institute of Physics, Ss. Cyril and Methodius University in Skopje, Faculty
of Natural Sciences and Mathematics-Skopje, Arhimedova 3, Skopje, 1000,
Republic of Macedonia*

Abstract. We present the R-band lightcurves of the Flora family asteroid
(12499) 1998 FR47, obtained in 2022 at two different astronomical sites: Bulgarian National Astronomical Observatory Rozhen (MPC Code 071) and Astronomical Station Vidojevica (MPC Code C89). The quadramodal lightcurves
reveal a rotation period of 6.172±0.003 h and an amplitude of about 0.44 mag.
Using the lightcurve inversion method, with the combination of our dense
lightcurves and the sparse data from Gaia DR3, we found the sidereal period, an indication of a retrograde rotation of (12499) and its low-convex resolution shape. Nonetheless, the unusual shape of the quadramodal lightcurve
and its additional analysis reveals two possible periods, 3.0834±0.0085 h and
4.1245±0.0151 h, making the suspect that the asteroid might be a non-synchronised wide binary system. Spectral analysis of the asteroid using data from the
GAIA DR3 shows that it is either an M- or an L-type object and maybe a piece
of the first planetesimals to form in the Solar System protoplanetary disk. On
the other hand, (12499)'s dynamical properties indicate a significantly shorter
lifetime. The asteroid lies exactly on the chaotic border of the 7:4 mean motion resonance with Mars (7M:4), alternating between being in and out of it
for almost 190 Myrs. During 200 Myrs of integration, (12499) visited other resonances in the Flora family, but it never became a Near Earth Object (NEO).
Additional integration of fictive objects from the 7M:4 resonance showed a
possibility of transportation to the NEO region already at about 20 Myrs.

Key words: binary asteroid – (12499) 1998 FR47 – photometry – spectroscopy

1. Introduction

An asteroid lightcurve is constructed by the rotation of an irregular ellipsoidal shape. In the usual case, lightcurves during one rotational phase should have two maxima and two minima with slightly different depths. On the other hand, some asteroids have shown unusual lightcurve shapes, which may be caused by different albedo over their surfaces or irregular shapes. Lately, different observational techniques confirm that some of these irregular lightcurves shapes could be caused by the binary nature of the observed asteroids (Tedesco, 1979; Margot et al., 2015). In the last two decades, numerous studies of these asteroid binary systems have been done, and the estimation is that around 15 % of the Near Earth Asteroids (NEA's), with diameters greater than 0.3 km, belong to this class (Pravec et al., 2006). There are a few characteristics of the lightcurve that may suggest the possibility of a binary system. The most common one is the presence of two minima with different depths separated by a half phase, which is usually caused by mutual events like occultations and eclipses between the two components. Unfortunately, determining a binary system is not always straightforward. If the system is not positioned equatorially to the observer or the components of the binary are distinctly separated, these features will not be presented in the lightcurve.

The asteroid (12499) 1998 FR47 was discovered on 1998 March 20 by the LINEAR project in Soccoro (New Mexico, USA). According to the Asteroid Lightcurve Photometry Database (ALCDEF)[1] (Stephens & Warner, 2018; Warner et al., 2009), the calculated diameter of (12499) is 4.591 km, and the assumed albedo is 0.277 (Mainzer et al., 2019). A search of the Asteroid Lightcurve Database found no previously reported period for asteroid (12499). The only available information about the asteroid lightcurve was its amplitude of 0.4 mag, reported by Simpson et al. (2013).

The asteroid (12499) is located at about 2.21 AU in the inner main belt in the region of the Flora family (although its membership to the family is somewhat questionable). According to Nesvorny (2020) it belongs to the Flora family, while the AstDys database[2] denoted it as a background asteroid. This discrepancy can be explained by the fact that the Flora family does not have sharp boundaries, but it gradually fades into the background population (see e.g. Vokrouhlický et al. (2017); Dykhuis et al. (2014)). Nevertheless, here we study only one of its potential members in the same way we studied the asteroid (4940) Polenov (Vchkova Bebekovska et al., 2021).

[1] https://alcdef.org

[2] Available at https://newton.spacedys.com/astdys/

2. Observations and data reduction

Our first photometric observations of the asteroid (12499) 1998 FR47 were on 2022 Aug 18 and 19, at Bulgarian National Astronomical Observatory (BNAO) Rozhen (MPC Code 071), when our primary targets were long-term studied asteroids. The observations were performed with a 50/70 Schmidt telescope, equipped with an FLI PL 16803 4096×24096 CCD with $9\,\mu$m pixels. The next observations were conducted on 2022 Sep 23 and 24 at Astronomical Station (AS) Vidojevica (MPC Code C89) with 60 cm Cassegrain "Nedeljković" telescopes equipped with an SBIG STXL-6303 3072×2047 CCD with $9\,\mu$m pixels.

After light image reduction, aperture photometry of the asteroid and comparison stars were performed with the software program CCDPHOT[3] by Buie (1996). For the lightcurve analysis, we used the software package MPO Canopus v10.8.4.1 [4], which produces composite lightcurves, calculates rotational periods, provides the Fourier analysis fitting procedure, and estimates the amplitude of the lightcurve.

Table 1 presents the aspect data for (12499) for the observational sets and Fig. 1 shows the Phase Angle Bisector (PAB) longitude, PAB latitude, and phase angle distributions for dense and sparse photometric data. Dense data correspond to observations in Table 1 and sparse data correspond to 19 accurate photometric points from 31 December 2014 to 13 May 2017 from GAIA Data Release 3 (DR3). The phase angles of the sparse satellite data are between 19 and 32 degrees and the phase angles of our dense data fill the gap around the asteroid opposition.
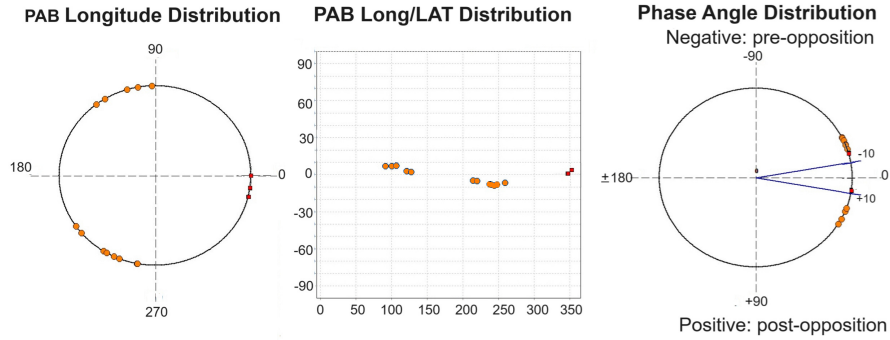
Figure 1. Dense (red points) and Gaia DR3 sparse observations (orange points). Left: Distribution of PAB longitude; Centre: Distribution of PAB longitude on PAB latitude; Right: Distribution of phase angle.

---

[3] https://www.boulder.swri.edu/~buie/idl/ccdphot.html
[4] https://minplanobs.org/BdwPub/php/mpocanopus.php

Table 1. Aspect data for the asteroid (12499) 1998 FR47 for the five observational sets.

Date[1] (UT)	r[2] (AU)	Δ[3] (AU)	Ph. angle[4] ($\alpha°$)	λ_e[5] (°)	β_e[6] (°)	MPC[7] code
2022 Aug 19.02	1.707	0.747	16.7016	355.04	0.26	071
2022 Aug 20.01	1.707	0.746	16.1411	354.96	0.40	071
2022 Sep 23.99	1.713	0.721	7.6643	348.70	5.12	C89
2022 Sep 24.04	1.713	0.721	7.7522	348.67	5.14	C89
2022 Sep 24.83	1.714	0.724	8.2522	348.53	5.22	C89

[1] The observation date referring to the mid-time of the lightcurve observed
[2] Heliocentric distance
[3] Geocentric distance
[4] The solar phase angle
[5] The J2000.0 ecliptic longitude
[6] The J2000.0 ecliptic latitude
[7] Minor Planet Centre Observatory Code
https://www.minorplanetcenter.net/iau/lists/ObsCodesF.html

3. Results

3.1. Lightcurve analysis

During the first night (12499) was observed for about 2.8 hours. By visual inspection of the typical asteroid bimodal symmetrical lightcurve, we thought that more than 90 % of its period was covered. To our surprise, the next night's observations with a duration of 4.5 h showed an asymmetrical lightcurve having three minima with different amplitudes. Combining these two nights' observations, we could not determine the rotational period.

During the next observations, carried out at AS Vidojevica, Sep 23 and 24, 2022, the solar phase angle of the asteroid was at 7.8° after opposition, and the asteroid was observed for about 8 and 4 hours, respectively. A Fourier fit of order 9 reveals an asymmetric quadramodal shape of the composite lightcurve and confirms a period of 6.172±0.003 h with an amplitude of 0.44±0.01 mag (see Fig. 2). Using the empirical relation between the amplitude and largest to the smallest axis ratio (a/c) proposed by Zappala et al. (1990) we computed a/c=1.39. Four well-defined maxima and minima with different heights could be due to an irregular shape of the asteroid and/or albedo variations on its surface.

This period was used in constructing the composite lightcurve from the previous observations, which were taken at a phase angle of 16.7° before opposition.
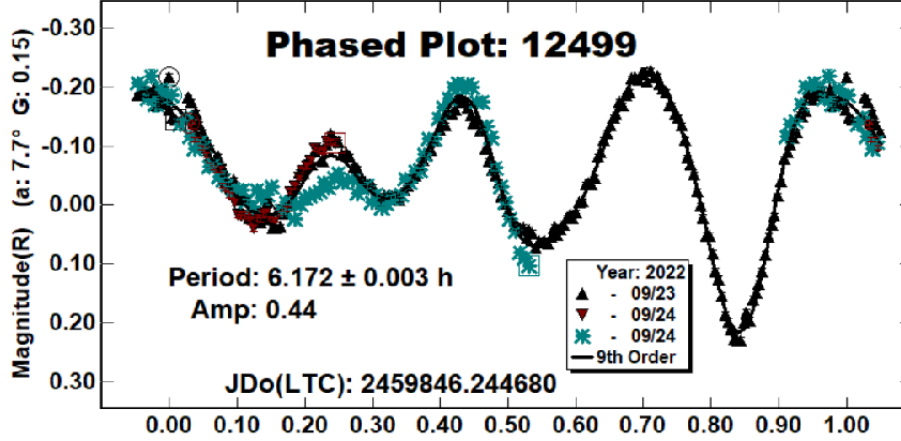
Figure 2. The composite lightcurve of (12499) 1998 FR47 gathered from the observations on 23 and 24 September 2020. The Fourier analysis of order 9 gave the best corresponding to the rotational period 6.172h±0.003 h with the amplitude of 0.44±0.01 mag.

Even though the data have a gap, the composite lightcurve constructed with a Fourier fit of order 6 again reveals an asymmetric quadramodal shape, that looks like a mirror image of the first composite lightcurve (see Fig. 3).

3.2. Testing a single-body shape model

Even though the irregular form of the observed lightcurve we decided to test for a single-body low-resolution shape model. For this purpose, we used the lightcurve inversion method (Kaasalainen & Torppa, 2001; Kaasalainen et al., 2001) and LCInvert programme part of the MPO Software[5]. Considering the tremendous accuracy of the DR3 photometric data we took the weighting factor to be set to 1.0 for both sparse and for dense photometric data. These sparse data added to our dense data give us a wide range of the PAB longitude distribution (see Fig. 1) which is very important for the shape reconstruction. We made the initial sidereal period search around our synodic period of 6.172 h (see Fig. 4–left panel). A narrower period search found a few solutions with 10 % of the lowest χ^2 (see Fig. 4–right panel), but we choose the one with the lowest χ^2, which is 6.16802461 h, as the most likely period and used it for the pole search.

The pole search produced 312 discrete and fixed pole positions distributed over the unit sphere with 15° steps in ecliptic latitude and longitude. The dark blue region in the constructed χ^2-map, presented in Fig. 5, has χ^2-value about

---

[5]https://minplanobs.org/BdwPub/php/displayhome.php
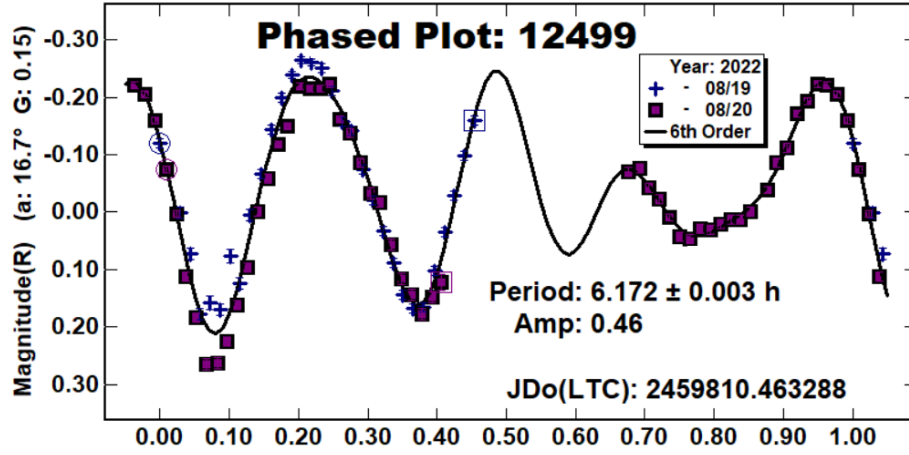
Figure 3. The lightcurve of (12499) 1998 FR47 gathered from the observations in August 2022. Although not completely covered, it is constructed on the basis of the afterwards calculated period of 6.172 h.
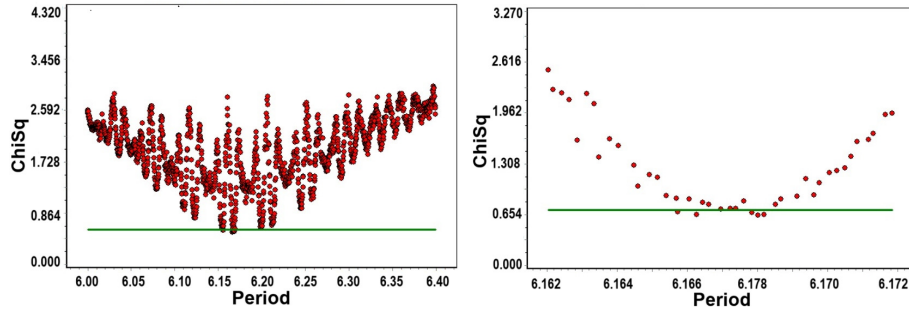
Figure 4. The periodograms of the initial sidereal period search around our synodic period of 6.172 h.

25 % smaller than χ^2-values of the dark red region. It corresponds to pole coordinates λ=300° and β=-60° and sidereal period 6.168027718 h. Taking those values as free parameters we made a finer pole search and we got sidereal period 6.16799606 h and pole coordinates λ=291.9° and β=-53.2°, which suggest the retrograde sense of the asteroid rotation. Assuming the triaxial ellipsoid form of the asteroid with axes a>b>c, which rotates around the shortest axis c=1, the calculated pole coordinates corresponded to the relative shape dimensions a/b=1.1 and a/c=1.3. The corresponding 3D shape model is also constructed and presented in Fig. 6. The comparison of the lightcurves generated from this

model with the dense lightcurves is shown in Fig.7. The modelled lightcurves in Fig.7 do not correspond well enough with the observations. These, together with the initial irregular form of the observed lightcurve, were indicators for searching for a double-period solution caused by the binary nature of the asteroid.
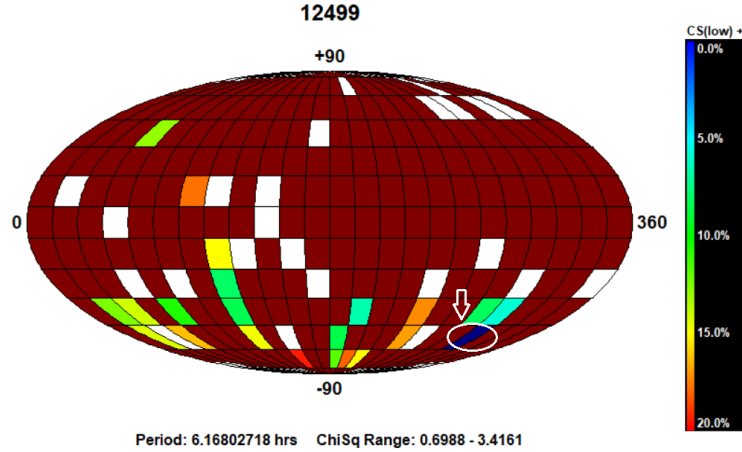

Figure 5. The χ^2-map of the pole search distribution. The white arrows indicate the dark blue region with the smallest value of χ^2. The dark blue regions have χ^2 values about 20% smaller than χ^2 values of the dark red regions.

3.3. Possible binary system

The complex form of the lightcurves, the unusual depth of one of the minima, as well as the diameter of the asteroid (smaller than 10 km), suggest that there could be two additive components in the lightcurve and that (12499) could be a candidate for a binary asteroid (Pravec et al., 2019). Using a Dual-period search (Warner, 2016) in MPO Canopus, we calculated the rotational period of the synodic period of both components. The first one has a period of 3.0834±0.0085 h and an amplitude of 0.27 mag and is presented in Fig. 8. The second one is with a period of 4.1245±0.0151 h and an amplitude of 0.22 mag and is presented in Fig. 9. Unfortunately, our observations did not capture any superimposed mutual events, and the distance between the two bodies is not constrained. The orbital period of the satellite using the data from these events could not be determined, which suggests that it may be a wide binary system.

Additional data from our observations and data from observers sufficiently far away in longitude are needed to cover the orbital period with mutual events (i.e. occultations and/or eclipses). It will help not only to decide if (12499) is a binary asteroid but also to refine our calculated periods for the primary and
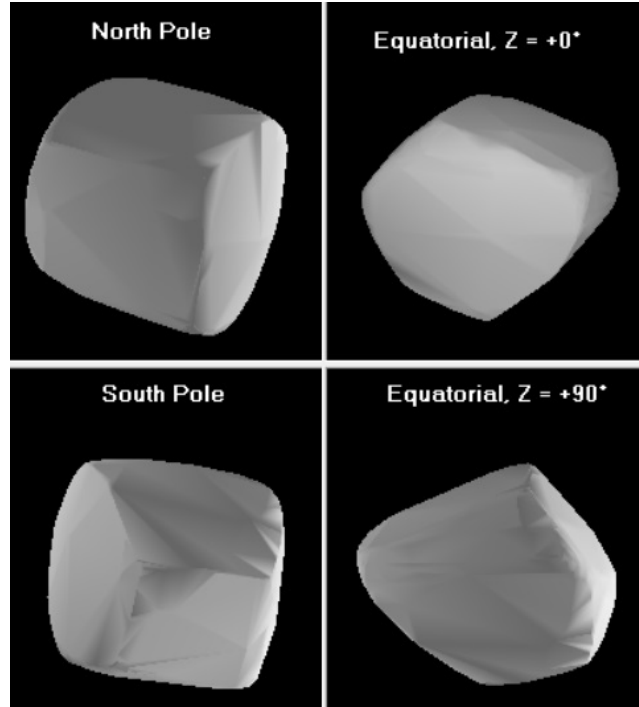
Figure 6. The 3D low-resolution convex shape model of (12499) 1998 FR47. The north and south pole views are given in two left panels, while the equatorial viewings with rotational phases 90° apart are given in two right panels. The calculated aspect ratio of the longest to two shorter semi-axis is a/b=1.1 and a/c=1.3.

for the secondary, as well as to determine the orbital period of the system. The best way is to organise an observational campaign on this object in the future.

3.4. Taxonomy from Gaia spectroscopy

The Gaia mission has been observing Solar System objects since the beginning of its operation. The Gaia DR3 includes, for the first time, the mean reflectance spectra of selected asteroids. Considering that (12499) is among them, we will use that data to further investigate its properties in the direction of taxonomy and composition, relying on the new probabilistic approach by Mahlke et al. (2022).

The results are shown in Fig. 10. The left panel shows the Gaia DR3 reflectance spectra of the object, the middle panel points out its latest published albedo obtained by NEOWISE (Mainzer et al., 2019), and the right panel presents the possible taxonomy classes with their probabilities.
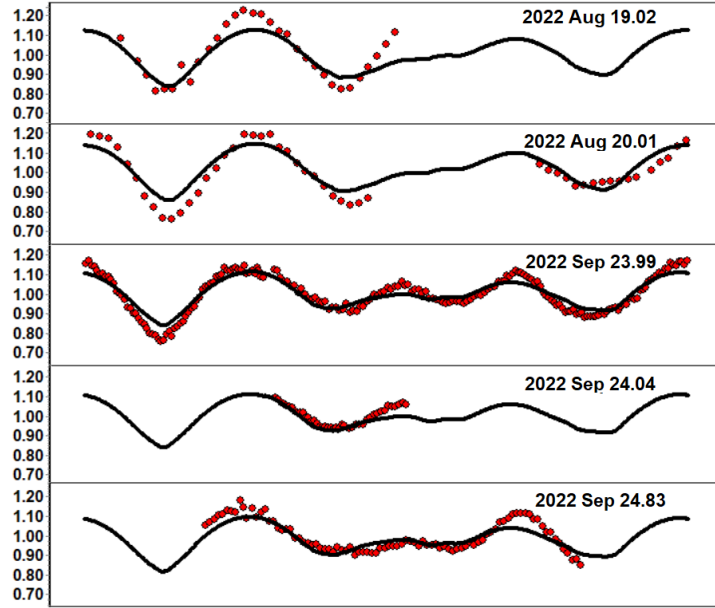
Figure 7. The lightcurve (red points) obtained from our dense observations superimposed over the lightcurves generated by the model constructed using a combination of our dense and GAIA DR3 sparse data.

In particular, the asteroid has a 66 % probability of being an M-class object and 30 % for an L-class. Both of these solutions fall into very diverse classes situated between primitive carbonaceous C- and silicate (partially thermally metamorphosed) S-classes (Cloutis et al., 1990, 2011; Vernazza et al., 2014). Other low probability solutions are 3 % for being an S-type object and 1 % for E-type.

The most probable M-class, which according to Mahlke et al. (2022) corresponds to the old Tholen (1984) M-class or the newest Bus-DeMeo (Bus & Binzel, 2002; DeMeo et al., 2009) Xk-class. Its reflectance spectrum has a linear red slope and possible faint features around $0.9\,\mu$m. The objects of this class are associated with at least two populations, the chondritic and the metallic (Vernazza et al., 2011; Viikinkoski et al., 2017), whose composition can vary, depending on their distance from the Sun and the time of format. The most probable formation scenario for M-type objects is that they are formed from a differentiated parent body after a collision and the fragments from the core, which were rich in metals, were formed them.

On the other hand, the reflectance spectrum of L-class asteroids is variable apart from a red visible slope and a small feature around $1\,\mu$m (Sunshine et al.,
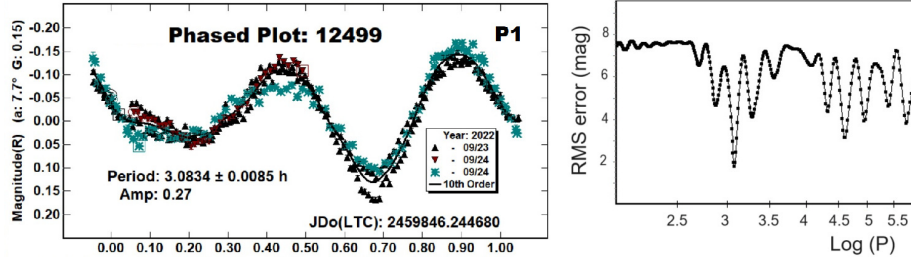
Figure 8. (12499) 1998 FR47 – the lightcurve of the primary (left panel) and the corresponding dual-period search periodogram (right panel).
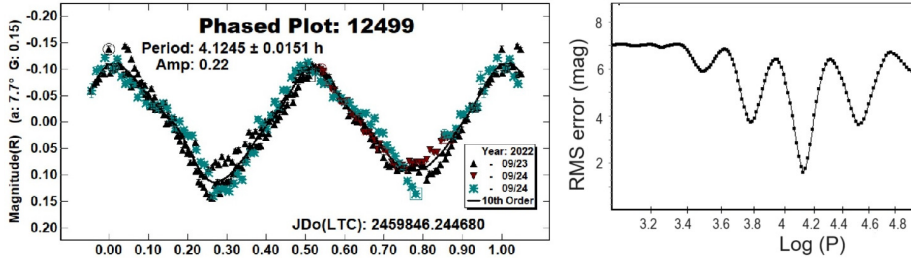

Figure 9. (12499) 1998 FR47 – the lightcurve of the secondary (left panel) and the corresponding dual-period search periodogram (right panel).

2008). The composition of this type of object is associated with large abundances of spinelbearing calcium–aluminium-rich inclusions, suggesting they may be pieces of the first planetesimals to form in the Solar System's protoplanetary disk (Devogèle et al., 2018).

3.5. Dynamical properties

Let us first remark that (12499)'s membership to the Flora family indirectly suggests that (12499) could be stable in long times, since the age of the family is estimated to $\sim 1\,\mathrm{Gyr}$ (Hanuš et al., 2013; Dykhuis et al., 2014; Brož et al., 2013). We will verify these stability assumptions in two ways: (a) by mapping and studying the orbital neighbourhood of the asteroid (b) by tracking the evolution of (12499) and several fictive objects in its close neighbourhood.

The calculation of maps is performed using the Fast Lyapunov Indicator - FLI (Froeschlé et al., 1997), a numerical tool which is efficient in dynamical cartography of both realistic (Daquin et al., 2016, 2022; Rosengren et al., 2017; Todorović, 2020, 2017) and idealised systems (Froeschlé et al., 2000). FLI values and the orbital evolution of individual test particles (TPs) are obtained
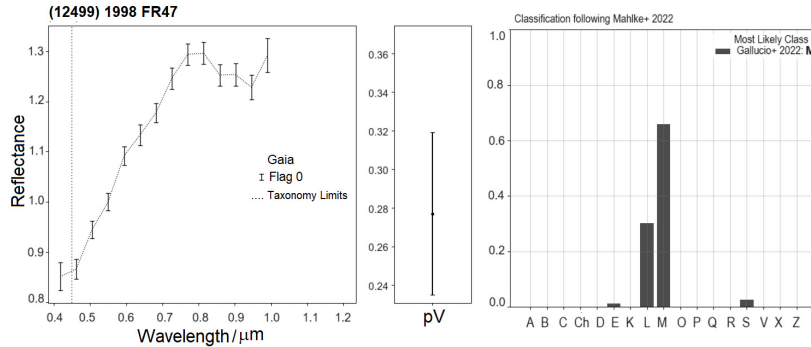
Figure 10. Gaia DR3 reflectance spectrum of (12499) 1998 FR47 and its taxonomical classification according to Mahlke et al. (2022) (see text for details).

with the orbit9 integrator available at http://adams.dm.unipi.it/orbfit/. We consider the gravitational influences of seven planets from Venus to Neptune. The mass of Mercury is added to the mass of the Sun, and a proper barycentric correction is applied. The non-gravitational Yarkovsky and YORP effects are not included in the calculation. In the integration, asteroids are treated as massless test particles. We do not consider their sense of rotation, nor the eventual mutual gravitational effect of the components in the possible binary system.

Fig. 11 shows one segment of the semi-major axis eccentricity (a, e) plane around the asteroid (12499). It is produced by taking $250\,000$ TPs regularly distributed on a 500×500 grid in $[a, e] = [2.18, 2.24] \times [0.15, 0.35]$. For each TP we calculate its corresponding FLI for 5000 years. Stable orbits have lower FLIs and are marked with dark blue colours, while the more chaotic ones have higher FLIs and are coloured with lighter shades of blue. The four remaining orbital elements, the inclination i, the longitude of the node Ω, the argument of the pericentre ω, and the mean anomaly M, are equal to the corresponding elements of (12499) for the epoch 2458800.5 MJD (13. November 2019). Their values are taken from the JPL NASA database[6] and are approximately $(i, \Omega, \omega, M) \sim (6.76°, 337.11°, 6.71°, 53.79°)$. By using this mapping method, we can see the realistic dynamical environment of (12499).

The map in Fig. 11 shows a large number of mean motion resonances (MMRs) appearing as vertical thin V-shaped structures. Additional calculations (not shown here) verified that most of them are resonances with Mars, confirming the domination of such resonances in the Flora family (Vokrouhlický et al., 2017; Nesvorný et al., 2002).

The location of the asteroid (12499) at $(a, e) = (2.21209, 0.23150)$ is marked with a white dot, while the green diamond shape at $(a, e) = (2.18289, 0.15945)$

---

[6]Available at https://ssd.jpl.nasa.gov/
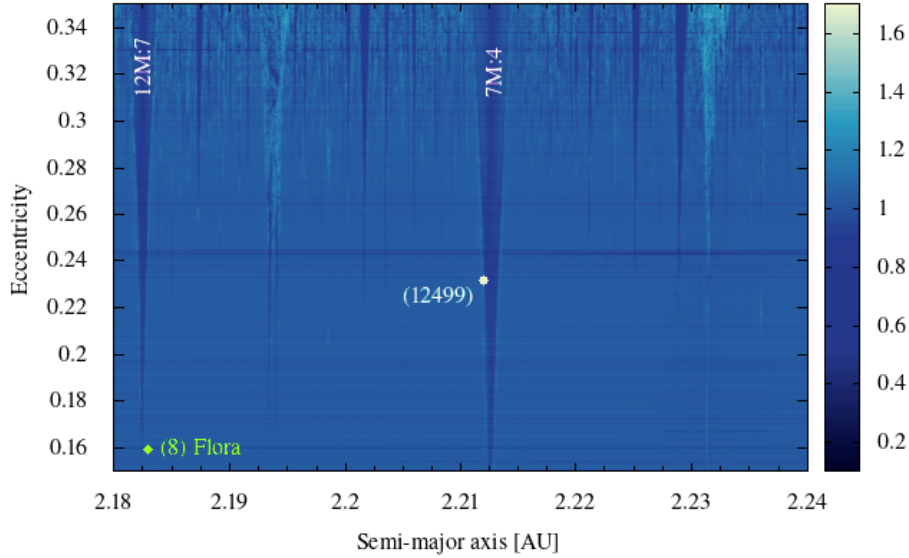
Figure 11. The 5000 years FLI map calculated in the semi-major axis, eccentricity plane for $[a, e] = [2.18, 2.24] \times [0.15, 0.35]$, where most of the vertical V-shaped structures are mean motion resonances with Mars. The asteroid (12499), marked with a white dot, lies close to the 7M:4 MMR at $a \sim 2.212$ AU. The position of the asteroid (8) Flora, the largest body in the family, is marked with a green diamond-like shape close to the 12M:7 MMR at about $a \sim 2.182$ AU.

shows the position of the asteroid (8) Flora, the possible largest remnant of the parent body of the family. Although our paper focuses on the asteroid (12499), we will make some other remarks on Fig. 11. Vokrouhlický et al. (2017) showed that the asteroid (8) Flora is close to the ν_6 and ν_{16} secular resonances[7]. Their presence is not visible on our map since it would require much longer integration times than 5000 yrs used here (see Todorović & Novaković (2015) for the detection of secular resonance in FLI maps). In Fig. 11 it appears that (8) Flora is close to the 12:7 MMR with Mars at about $a \sim 2.182$ AU (for the identification of mean motion resonances see e.g. Gallardo (2006); Smirnov (2023)). Still, its exact distance from the 12M:7 resonance as visible on the chart, is not entirely reliable, since the map illustrates the dynamical situa-

---

[7]Resonances ν_6 and ν_{16} occur when the precession and nodal frequencies of the asteroid's orbit equal the precession and nodal frequencies of the orbit of Saturn, respectively.
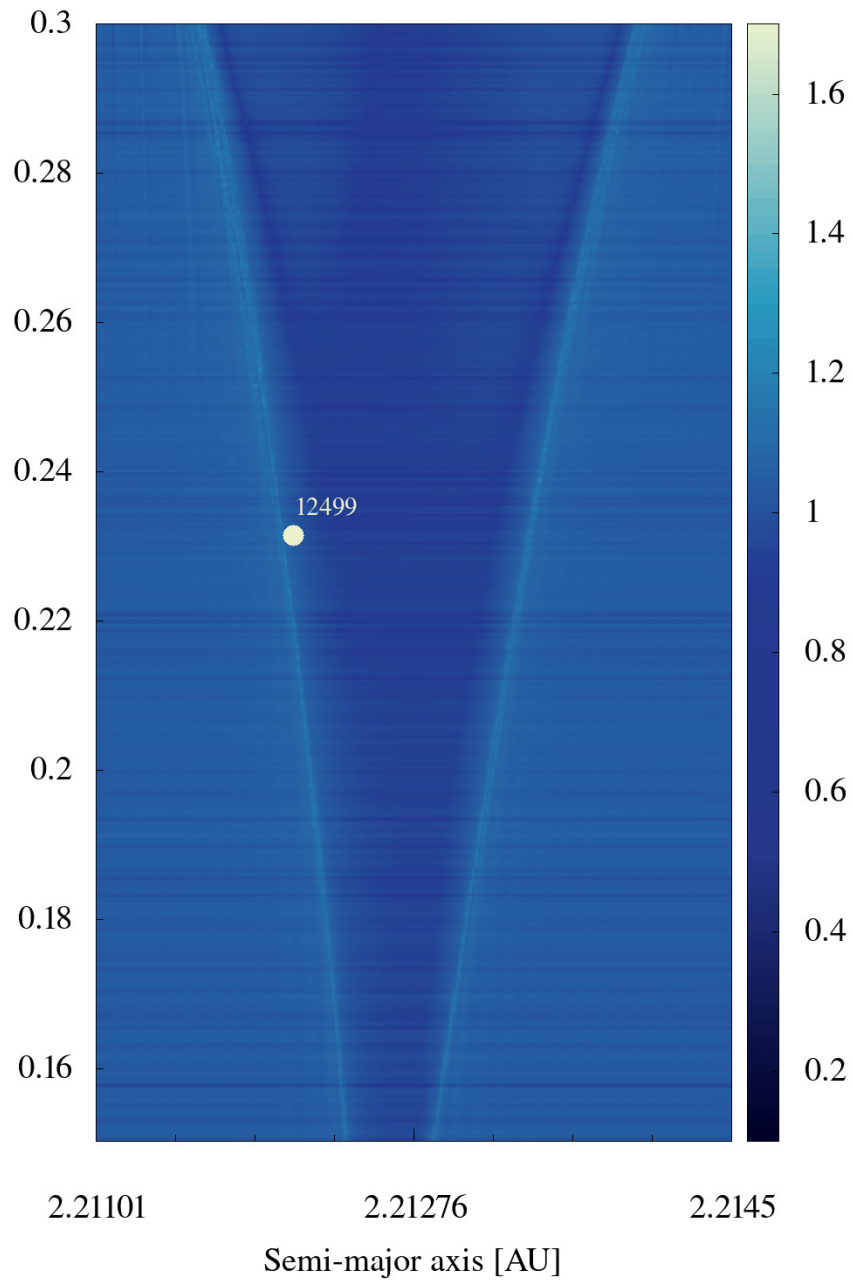
tion in the orbital plane of the asteroid (12499). The shape and the positions of resonances change with the change of orbital angles, and according to the JPL database for the particular epoch, (8) Flora is 199.6 degrees in front of (12499) in the mean anomaly M, it has 226.2 degrees larger longitude of the node Ω, and is 79.6 degrees behind in the argument of pericentre ω, id est $M_{(8)} - M_{(12499)} = 199.6°, \Omega_{(8)} - \Omega_{(12499)} = 226.2°, \omega_{(8)} - \omega_{(12499)} = -79.6°$.

In Fig. 11 the asteroid (12499) is placed at the 7:4 mean motion resonance with Mars. In a closer look given in Fig. 12, for $[a, e] = [2.21101, 2.2145] \times [0.15, 0.3]$, we notice that (12499) lies exactly on the chaotic border of the resonance.

Several asteroid pairs are already associated with mean motion resonances (see for example Pravec et al. (2019), Duddy et al. (2012), or Rosaev (2024)). We are unaware that any such pair is found on the very edge of resonance, as is the case for (12499). It remains an open question whether the position on the resonant border may be related to the duality (binarity) of the asteroid.

In the following part, we will verify the long-term stability of (12499). In Fig. 13 we show two perspectives of its orbital evolution during 200 Myrs. The top panel shows which parts of the (a, e) plane are visited by (12499), where its trace is coloured pink. The lower panel gives the change of (12499)'s semi-major axis $a_{(12499)}$ during the integration time. The value of $a_{(12499)}$ remains close to the centre of the 7M:4 resonance at ~ 2.212 AU for about 190 Myrs, after which it starts an excursion to nearby resonances, but inside the family. We use the rough boundaries of the Flora family from Nesvorný et al. (2002) which are $2.12 < a < 2.31$ AU, $0.11 < e < 0.175$, and $3 < i < 7.5°$. The (12499)'s perihelion distance q reached Mars crossing values ($q = 1.665$ AU) several times, for the first time after about 0.6 Myrs. However, (12499) did not become a Near Earth Object ($q < 1.3$ AU) since its minimal perihelion distance was about $q \sim 1.4$ AU.

Another look at (12499)'s evolution for $t \in [50, 155]$ Kyrs is given in Fig. 14. On the top plot, we track the critical angle of (12499) for the 7M:4 resonance defined with $\sigma_{7M:4} = 7\lambda_a + 4\lambda_M - 3\tilde{\omega}_a$, where λ_a and λ_M are the mean longitudes of the asteroid and Mars respectively, (defined with $\lambda = M + \omega + \Omega$), while $\tilde{\omega}_a$ is the asteroids longitude of perihelion $\tilde{\omega} = \omega + \Omega$. The lower panel shows the evolution of $a_{(12499)}$ for the same time. We notice that $\sigma_{7M:4}$ and $a_{(12499)}$ have synchronised changes. In the first 80 Kyrs, $\sigma_{7M:4}$ librates, and $a_{(12499)}$ oscillates, meaning the asteroid is trapped in the resonance. In the next 70 Kyrs the asteroid is outside the resonance since the critical angle circulates (it has smooth changes in the $[0, 360]$ interval), while $a_{(12499)}$ is almost constant. The next entry in the 7M:4 resonance starts at ~ 130 Kyrs and lasts for about 20 Kyrs. Such alternating episodes of going in and out of the resonance are observed for 190 Myrs. In Fig. 14 we plotted a relatively short time interval of about ~ 100 Kyrs (between $t \in [50, 155]$ Kyrs), because the fine oscillations in $\sigma_{7M:4}$ and $a_{(12499)}$ are not noticeable for a 200 Myrs interval (see panel b in Fig. 13).

Figure 12. The enlarged portion of Fig. 11 around the 7M:4 resonance for $[a, e] = [2.21101, 2.2145]$ AU $\times [0.15, 0.3]$. The asteroid (12499), marked with the white dot, is located exactly on the chaotic border of the resonance.
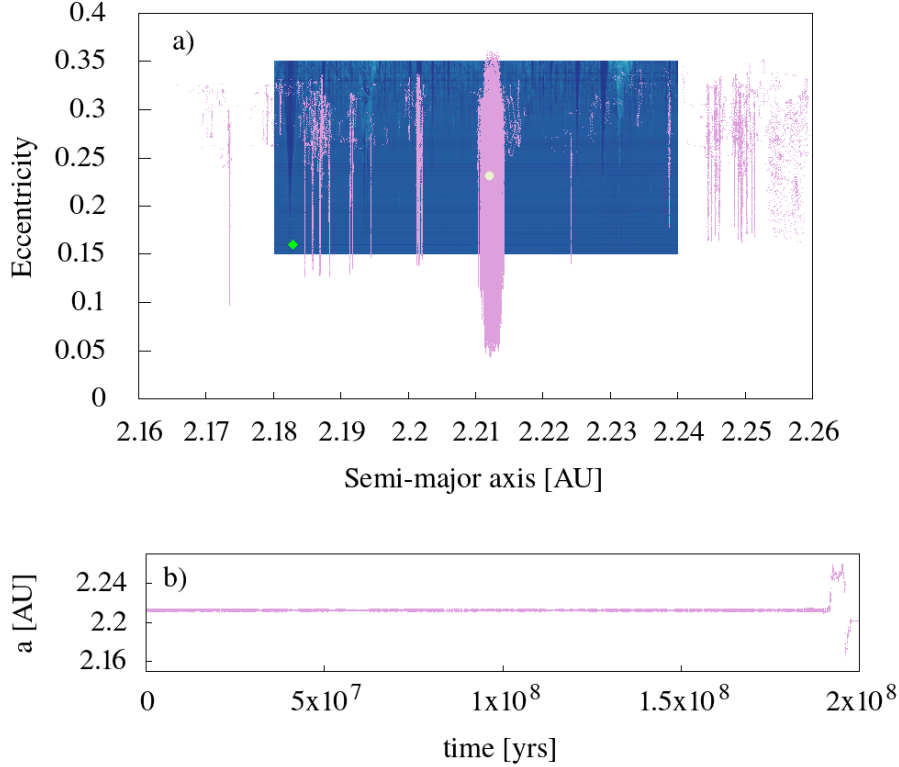
Figure 13. The top panel shows the orbital evolution of (12499) in the (a, e) plane during 200 Myrs of integration. The places visited by the asteroid are coloured pink. The map from Fig. 11 is set in the background for better orientation. In addition to the 7M:4 resonance at $a \sim 2.212$ AU (from which it originated), (12499) visited numerous neighbouring resonances but did not leave the Flora family. The lower panel shows the evolution of $a_{(12499)}$ during the whole integration time. The asteroid remains close to (or inside) the 7M:4 resonance at $a \sim 2.212$ AU for almost 190 Myrs. Its excursion to the neighbouring MMRs occurred in the last 10 Myrs of integration.

In the end, we selected 20 additional TPs from the chaotic border of the 7M:4 MMR from Fig. 12 and observed their orbital evolution in 50 Myrs. Assuming (12499) could be a binary asteroid lying on the chaotic border of a resonance, we may expect that initially close segments could have a large orbital divergence. We emphasise again that we did not treat the gravitational interaction between the possible components of the binary, but only the evolution of individual massless TPs in the above-described Solar system model.
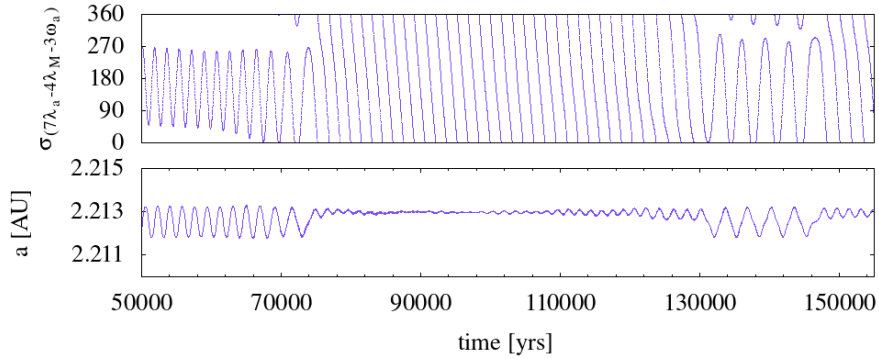
Figure 14. The change of (12499)'s critical angle for the 7M:4 MMR $\sigma_{7M:4}$ (top panel) and the change of its semi-major axis $a_{(12499)}$ (bottom panel) for $t \in [50, 155]$ Kyrs. The asteroid spent around 72 Kyrs librating in the resonance (the first 50 Kyrs are not presented). In the next 80 Kyrs i.e. until ~ 130 Kyrs, $\sigma_{7M:4}$ circulates, meaning the asteroid was pushed out of the resonance, but not far since its semi-major axis has a quasi-constant value close to the resonance at about $a_{(12499)} \sim 2.213\,AU$. Another episode of libration in $\sigma_{7M:4}$ and oscillation in $a_{(12499)}$ occurred between 130 and 150 Kyrs, meaning the asteroid is trapped in the resonance again. We observed that such libration-oscillation modes in $\sigma_{7M:4}$ alternate for about 190 million years.

The results of this last set of integration are given in Fig. 15. Again, we show the (a, e) plane but for a larger domain for $[a, e] = [0, 100]$AU $\times [0, 1]$, where the semi-major axis is presented on the logarithmic scale. This portion of the (a, e) plane was selected because we observed large-scale changes in the orbital elements of the test asteroids. More precisely, 4 among the 20 objects experienced macroscopic evolution through the Solar system. These four asteroids were thrown out of the resonance by close approaches with Mars, followed by a series of encounters with Earth and Venus. Only one among the four test objects had an approach with Jupiter. The resulting orbital pathways in the (a, e) plane are coloured in red (Fig. 15). We notice they spread mostly between the apsidal lines of Jupiter q_J and Q_J (marked with two grey lines). The first entries in the NEO region are observed at about 20 Myrs, in significantly shorter times than the average deliveries of 100 Myrs as reported in Nesvorný et al. (2002). The remaining 16 test asteroids stayed in the 7M:4 resonance; their trace in the chart at about 2.21 AU, is coloured green. Let us mention that this result represents a possible outcome of the chaotic evolution, whereas, in reality, we could expect shorter evolution timescales, due to eventual close approaches with the largest asteroids and/or nongravitational effects like YORP and Yarkovsky.

Our results show that the Flora family is efficient in supplying the NEO region also through weak MMRs with Mars, not only via the ν_6 resonance as a

main driver. Still, we emphasise that this last set of test asteroids is intentionally chosen from the resonant chaotic border, meaning the real possibilities for this scenario are somewhat lower, but not impossible.
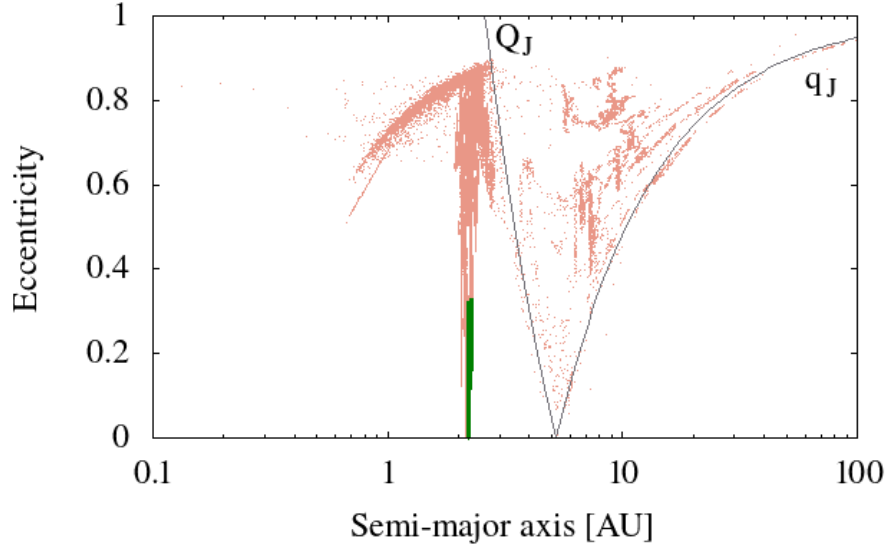
Figure 15. The trace of 20 test asteroids initially placed on the borders of the 7:4 MMR with Mars, during 50 Myrs of orbital evolution. We cover a large segment of the Solar system $[a, e] = [0, 100] \, \mathrm{AU} \times [0, 1]$, where the semi-major axis is given in the $\log_{10}$ scale. Among the 20 test objects, four of them were thrown out of resonance due to close approaches with Mars (and other inner planets), entered the NEO region and experienced a macroscopic diffusion through the Solar system (their traces are coloured red). The 16 remaining bodies stayed close to the 7M:4 MMR around $a \sim 2.212 \, \mathrm{AU}$. Their trace in the chart is coloured green. The two apsidal lines of Jupiter q_J and Q_J are marked with thin light grey lines.

4. Conclusions

The unusual shape of the observed lightcurve for the asteroid (12499) 1998 FR47 was investigated in different senses. Firstly we try to determine the rotational period, axis poles, and shape of the object assuming a single body. The

solution suggests a rare quadramodal shape of the lightcurve with a rotational period of 6.172±0.003 h and an unusual shape to model it. Then we saw that the lightcurve can be modelled by two different periods and performed a dual-period search assuming that the asteroid is a binary system. The two solutions are 3.0834±0.0085 h and 4.1245±0.0151 h respectively for the primary and secondary bodies. No mutual event was detected in the lightcurve, so we suppose that these periods are of the individual lightcurves of the two bodies of the system, which is not synchronised and most probably is a wide binary system.

The available Gaia DR3 reflectance spectrum of the object suggests either M- or L-type taxonomy. They both are from the M-complex and suggest either chondritic or metallic composition or an object with large abundances of spinelbearing calcium–aluminium-rich inclusions, suggesting that the asteroid (12499) might be a piece of the first planetesimals to form in the Solar System protoplanetary disk.

Dynamical studies showed that (12499) is located at the very edge of the 7:4 mean motion resonance with Mars, where it should spend the next 190 Myrs, after which it should start a tour of nearby resonances. Additional calculations showed that TPs on the chaotic border of the 7M:4 MMR, close to (12499), may experience shorter stays in the resonance and faster deliveries to the NEO region and/or macroscopic diffusion starting already at 20 Myrs. Since our model does not include Yarkovsky or YORP effects, there is a possibility that the reported times are even shorter.

References

Brož, M., Morbidelli, A., Bottke, W. F., et al., Constraining the cometary flux through the asteroid belt during the late heavy bombardment. 2013, *Astronomy and Astrophysics*, **551**, A117, DOI: 10.1051/0004-6361/201219296

Buie, M. W., CCDPHOT—An IDL Widget Based CCD Photometry Reduction System. 1996, in Astronomical Society of the Pacific Conference Series, Vol. **101**, *Astronomical Data Analysis Software and Systems V*, ed. G. H. Jacoby & J. Barnes, 135

Bus, S. J. & Binzel, R. P., Phase II of the Small Main-Belt Asteroid Spectroscopic Survey. A Feature-Based Taxonomy. 2002, *Icarus*, **158**, 146, DOI: 10.1006/icar.2002.6856

Cloutis, E. A., Gaffey, M. J., Smith, D. G. W., & Lambert, R. S. J., Metal Silicate Mixtures: Spectral Properties and Applications to Asteroid Taxonomy. 1990, *Journal of Geophysics Research*, **95**, 8323, DOI: 10.1029/JB095iB06p08323

Cloutis, E. A., Hudon, P., Hiroi, T., Gaffey, M. J., & Mann, P., Spectral reflectance properties of carbonaceous chondrites: 2. CM chondrites. 2011, *Icarus*, **216**, 309, DOI: 10.1016/j.icarus.2011.09.009

Daquin, J., Legnaro, E., Gkolias, I., & Efthymiopoulos, C., A deep dive into the 2 g +h resonance: separatrices, manifolds and phase space structure of navigation satellites. 2022, *Celestial Mechanics and Dynamical Astronomy*, **134**, 6, DOI: 10.1007/s10569-021-10060-6

Daquin, J., Rosengren, A. J., Alessi, E. M., et al., The dynamical structure of the MEO region: long-term stability, chaos, and transport. 2016, *Celestial Mechanics and Dynamical Astronomy*, **124**, 335, DOI: 10.1007/s10569-015-9665-9

DeMeo, F. E., Binzel, R. P., Slivan, S. M., & Bus, S. J., An extension of the Bus asteroid taxonomy into the near-infrared. 2009, *Icarus*, **202**, 160, DOI: 10.1016/j.icarus.2009.02.005

Devogèle, M., Tanga, P., Cellino, A., et al., New polarimetric and spectroscopic evidence of anomalous enrichment in spinel-bearing calcium-aluminium-rich inclusions among L-type asteroids. 2018, *Icarus*, **304**, 31, DOI: 10.1016/j.icarus.2017.12.026

Duddy, S. R., Lowry, S. C., Wolters, S. D., et al., Physical and dynamical characterisation of the unbound asteroid pair 7343-154634. 2012, *Astronomy and Astrophysics*, **539**, A36, DOI: 10.1051/0004-6361/201118302

Dykhuis, M. J., Molnar, L., Van Kooten, S. J., & Greenberg, R., Defining the Flora Family: Orbital properties, reflectance properties and age. 2014, *Icarus*, **243**, 111, DOI: 10.1016/j.icarus.2014.09.011

Froeschlé, C., Guzzo, M., & Lega, E., Graphical Evolution of the Arnold Web: From Order to Chaos. 2000, *Science*, **289**, 2108, DOI: 10.1126/science.289.5487.2108

Froeschlé, C., Lega, E., & Gonczi, R., Fast Lyapunov Indicators. Application to Asteroidal Motion. 1997, *Celestial Mechanics and Dynamical Astronomy*, **67**, 41, DOI: 10.1023/A:1008276418601

Gallardo, T., Atlas of the mean motion resonances in the Solar System. 2006, *Icarus*, **184**, 29, DOI: 10.1016/j.icarus.2006.04.001

Hanuš, J., Brož, M., Durech, J., et al., An anisotropic distribution of spin vectors in asteroid families. 2013, *Astronomy and Astrophysics*, **559**, A134, DOI: 10.1051/0004-6361/201321993

Kaasalainen, M. & Torppa, J., Optimization Methods for Asteroid Lightcurve Inversion. I. Shape Determination. 2001, *Icarus*, **153**, 24, DOI: 10.1006/icar.2001.6673

Kaasalainen, M., Torppa, J., & Muinonen, K., Optimization Methods for Asteroid Lightcurve Inversion. II. The Complete Inverse Problem. 2001, *Icarus*, **153**, 37, DOI: 10.1006/icar.2001.6674

Mahlke, M., Carry, B., & Mattei, P. A., Asteroid taxonomy from cluster analysis of spectrometry and albedo. 2022, *Astronomy and Astrophysics*, **665**, A26, DOI: 10.1051/0004-6361/202243587

Mainzer, A. K., Bauer, J. M., Cutri, R. M., et al., NEOWISE Diameters and Albedos V2.0. 2019, *NASA Planetary Data System*, DOI: 10.26033/18S3-2Z54

Margot, J. L., Pravec, P., Taylor, P., Carry, B., & Jacobson, S., Asteroid Systems: Binaries, Triples, and Pairs. 2015, in *Asteroids IV* (University of Arizona Press), 355–374

Nesvorny, D., Nesvorny HCM Asteroid Families V1.0. 2020, *NASA Planetary Data System*, urn:nasa:pds:ast.nesvorny.families::1.0

Nesvorný, D., Morbidelli, A., Vokrouhlický, D., Bottke, W. F., & Brož, M., The Flora Family: A Case of the Dynamically Dispersed Collisional Swarm? 2002, *Icarus*, **157**, 155, DOI: 10.1006/icar.2002.6830

Pravec, P., Fatka, P., Vokrouhlický, D., et al., Asteroid pairs: A complex picture. 2019, *Icarus*, **333**, 429, DOI: 10.1016/j.icarus.2019.05.014

Pravec, P., Scheirich, P., Kušnirák, P., et al., Photometric survey of binary near-Earth asteroids. 2006, *Icarus*, **181**, 63, DOI: 10.1016/j.icarus.2005.10.014

Rosaev, A., Resonant perturbation of a family of young asteroids associated with (5026) Martes. 2024, *arXiv e-prints*, arXiv:2403.03559, DOI: 10.48550/arXiv.2403.03559

Rosengren, A. J., Daquin, J., Tsiganis, K., et al., Galileo disposal strategy: stability, chaos and predictability. 2017, *Monthly Notices of the RAS*, **464**, 4063, DOI: 10.1093/mnras/stw2459

Simpson, G., Chong, E., Gerhardt, M., et al., Asteroid Lightcurve Analysis at the Oakley Southern Sky Observatory: 2012 August - October. 2013, *Minor Planet Bulletin*, **40**, 146

Smirnov, E. A., A new python package for identifying celestial bodies trapped in mean-motion resonances. 2023, *Astronomy and Computing*, **43**, 100707, DOI: 10.1016/j.ascom.2023.100707

Stephens, R. & Warner, B. D., The ALCDEF Database and the NASA SBN/PDS: The Perfect Merger. 2018, in AAS/Division for Planetary Sciences Meeting Abstracts, Vol. **50**, *AAS/Division for Planetary Sciences Meeting Abstracts #50*, 417.03

Sunshine, J. M., Connolly, H. C., McCoy, T. J., Bus, S. J., & La Croix, L. M., Ancient Asteroids Enriched in Refractory Inclusions. 2008, *Science*, **320**, 514, DOI: 10.1126/science.1154340

Tedesco, E. F., Binary Asteroids: Evidence for Their Existence from Lightcurves. 1979, *Science*, **203**, 905, DOI: 10.1126/science.203.4383.905

Tholen, D. J. 1984, Asteroid Taxonomy from Cluster Analysis of Photometry., PhD thesis, University of Arizona

Todorović, N., The precise and powerful chaos of the 5:2 mean motion resonance with Jupiter. 2017, *Monthly Notices of the RAS*, **465**, 4441, DOI: 10.1093/mnras/stw3070

Todorović, N., Mapping of the asteroid families. 2020, in *IAU General Assembly*, 17–18

Todorović, N. & Novaković, B., Testing the FLI in the region of the Pallas asteroid family. 2015, *Monthly Notices of the RAS*, **451**, 1637, DOI: 10.1093/mnras/stv1003

Vchkova Bebekovska, E., Todorović, N., Kostov, A., Donchev, Z., & Borisov, G., The Physical and Dynamical Characteristics of the Asteroid 4940 Polenov. 2021, *Serbian Astronomical Journal*, **202**, 39, DOI: 10.2298/SAJ2102039V

Vernazza, P., Lamy, P., Groussin, O., et al., Asteroid (21) Lutetia as a remnant of Earth's precursor planetesimals. 2011, *Icarus*, **216**, 650, DOI: 10.1016/j.icarus.2011.09.032

Vernazza, P., Zanda, B., Binzel, R. P., et al., Multiple and Fast: The Accretion of Ordinary Chondrite Parent Bodies. 2014, *Astrophysical Journal*, **791**, 120, DOI: 10.1088/0004-637X/791/2/120

Viikinkoski, M., Hanuš, J., Kaasalainen, M., Marchis, F., & Ďurech, J., Adaptive optics and lightcurve data of asteroids: twenty shape models and information content analysis. 2017, *Astronomy and Astrophysics*, **607**, A117, DOI: 10.1051/0004-6361/201731456

Vokrouhlický, D., Bottke, W. F., & Nesvorný, D., Forming the Flora Family: Implications for the Near-Earth Asteroid Population and Large Terrestrial Planet Impactors. 2017, *Astronomical Journal*, **153**, 172, DOI: 10.3847/1538-3881/aa64dc

Warner, B. D. 2016, *A Practical Guide to Lightcurve Photometry and Analysis* (Springer Cham)

Warner, B. D., Harris, A. W., & Pravec, P., The asteroid lightcurve database. 2009, *Icarus*, **202**, 134, DOI: 10.1016/j.icarus.2009.02.003

Zappala, V., Cellino, A., Barucci, A. M., Fulchignoni, M., & Lupishko, D. F., An analysis of the amplitude-phase relationship among asteroids. 1990, *Astronomy and Astrophysics*, **231**, 548